Refinement of Asteroid Rotation Parameters via Stereo Intersection Angle Optimization and Masked Feature Matching

Zhen Peng [1,2], Xun Geng [1,2,*], Pengying Liu[1,2], Wenhao Liu[1,2], Haoyu Zhang[1,2]

[1] State Key Laboratory of Spatial Datum, Faculty of Geographical Science and Engineering, Henan University, Zhengzhou, China, 450046 (gengxun@henu.edu.cn);

[2] College of Geographic Sciences, Henan University, Zhengzhou, China, 450046.

Keywords: Asteroid Rotation Parameters, Intersection Angle Optimization, Grayscale Threshold Masking, Feature Matching

Abstract:

Determining accurate asteroid rotation parameters is essential for establishing a body-fixed coordinate system during deep-space proximity operations. However, early mission phases often lack prior exterior orientation data. When combined with edge effects from the deep-space background, this deficiency leads to high mismatch rates and ill-conditioned geometries. In this paper, we propose an integrated photogrammetric pipeline to refine these parameters using adaptive feature masking and stereo intersection angle optimization. Rather than using conventional matching, our approach isolates the asteroid target via an adaptive grayscale-threshold mask and morphological refinement, which restricts feature extraction to valid surface textures and significantly reduces outliers. We then introduce a geometric filter to discard stereo pairs with intersection angles below 5°, effectively preventing error propagation along the line of sight. Ultimately, the precise Right Ascension (RA) and Declination (Dec) are determined through an iterative coarse-to-fine grid search that minimizes spatial intersection residuals. Testing our method on 127 images of asteroid (162173) Ryugu from the Hayabusa2 ONC-T camera yielded strong results. The masking strategy successfully cut the number of mismatches in half (from 14,949 to 7,369). Within four iterations, the rotational parameters converged to RA = 96.5° and Dec = -66.4°. These refined results offer a reliable foundation for subsequent 3D reconstruction and high-precision planetary mapping.

1. Introduction

Asteroids preserve some of the earliest, untouched records of solar system formation. Consequently, exploring these bodies in-situ offers a unique window into our cosmic origins and primordial material composition (Watanabe et al., 2019). Yet, navigating and mapping these targets remains technically daunting. Spacecraft must operate in environments characterized by weak gravity, highly irregular topography, and complex orbital dynamics. Upon arriving at an unknown celestial body, the immediate priority is to establish a reliable body-fixed coordinate system to support all subsequent proximity operations. This requires determining the asteroid's precise rotational parameters—namely, the Right Ascension (RA) and Declination (Dec) of its pole. These parameters provide the strict mathematical foundation necessary to transform coordinates from the celestial inertial frame to the body-fixed frame.

When studying major celestial bodies, researchers routinely derive high-precision rotational parameters by analyzing extensive, long-term astronomical datasets. These datasets frequently incorporate diverse measurements, such as remote sensing imagery, continuous Doppler tracking, or laser altimetry (Folkner et al., 2018). Asteroids present a fundamentally different challenge. Because historical, long-term observational records for these smaller targets are notoriously sparse, scientists must rely on an alternative approach. During the critical early phases of an exploration mission, onboard optical images frequently serve as the absolute primary resource for estimating the object's spin state. While spacecraft approach their targets, various visual and navigational techniques come into play to calculate these dynamics. Prior to arrival, teams might utilize ground-based telescopes or orbital observatories to secure preliminary, baseline estimates of the asteroid's rotation. However, traditional techniques like light curve inversion inherently suffer from severe resolution constraints. The resulting coarse precision falls noticeably short of what modern missions actually demand, as both high-fidelity topographic mapping and safe, precise flight navigation require significantly tighter error margins.

This limitation is evident in several key studies. For (1) Ceres, (Drummond et al., 1998) derived a pole orientation with a right ascension (RA) of 333°±2° and a declination (Dec) of 43°±2°. Using imagery from the Hubble Space Telescope, (Thomas et al., 1997) determined the spin axis orientation of asteroid (4) Vesta to be RA=308°±10° and Dec=48°±10°. For near-Earth asteroid (162173) Ryugu, (Müller et al., 2017) employed light curve inversion techniques on data from the Herschel Space Observatory in combination with ground-based observations, estimating the spin axis orientation to lie within a right ascension range of approximately 310° to 340° and a declination of −40°±15° (Watanabe et al., 2019). Higher precision requires extensive photogrammetric analysis. In the case of comet 67P/Churyumov-Gerasimenko, a stereo-photogrammetric (SPG) analysis of 218 high-resolution OSIRIS images achieved a refined pole solution of RA=69.54°±0.1° and Dec=64.11°±0.05° (Preusker et al., 2015; Jorda et al., 2016)). Furthermore, an inertial frame bundle adjustment based on a control point network (Burmeister et al., 2018) derived from 8,010 image point measurements across 72 images (53 Mars Express and 19 Viking frames) yielded a spin axis orientation of RA=317.655°±0.025° and Dec=52.885°±0.019°.

Even with such progress in the field, refining an asteroid's spin state during the initial approach remains a formidable task. A primary hurdle is that the absolute exterior orientation—the exact spatial positioning and attitude of the spacecraft's cameras—is fundamentally unknown at this stage. If researchers attempt to force spatial intersections using stereo image pairs that share excessively narrow intersection angles, they inevitably create ill-

This contribution has been peer-reviewed.
https://doi.org/10.5194/isprs-archives-XLIX-B3-2026-1249-2026

conditioned geometric setups. Under these weak configurations, the slightest sub-pixel measurement error drastically magnifies, translating into massive depth displacements for the reconstructed 3D points along the camera's line of sight. Beyond these geometric pitfalls, the stark visual contrast of deep space introduces its own set of photometric problems. The sharp boundary separating the brightly illuminated celestial body from the surrounding pitch-black void consistently triggers severe edge effects. Vision algorithms frequently misinterpret these high-contrast borders, extracting swarms of spurious, unstable feature points. Because these false features severely lack descriptor distinctiveness and spatial consistency, they almost guarantee a high volume of mismatched correspondences during the critical feature tracking stage.

Building upon the preliminary exhaustive search evaluated by (Peng et al., 2025), we propose an advanced pipeline for refining asteroid rotation parameters. This method tightly integrates a rigorous grayscale masking strategy with the optimal selection of stereo intersection angles. By cleanly isolating the celestial body from the deep-space background and discarding weak viewing geometries, our approach actively suppresses false matches and intersection residuals. Ultimately, this enables high-precision refinement of the rotational parameters relying entirely on the visual data itself, bypassing the need for strict a priori constraints (Kuppa et al., 2022).

2. Method

To robustly refine the rotational parameters of asteroids from optical images without prior exterior orientation data, this paper proposes an integrated photogrammetric pipeline. The overall workflow consists of three main stages: (1) adaptive masking and morphological refinement to eliminate background interference, (2) spatial forward intersection and optimal selection of stereo pairs based on intersection angles, and (3) an iterative coarse-to-fine grid search to determine the optimal Right Ascension (RA) and Declination (Dec) by minimizing the intersection residuals. The complete flowchart of the proposed methodology is illustrated in Figure 1.

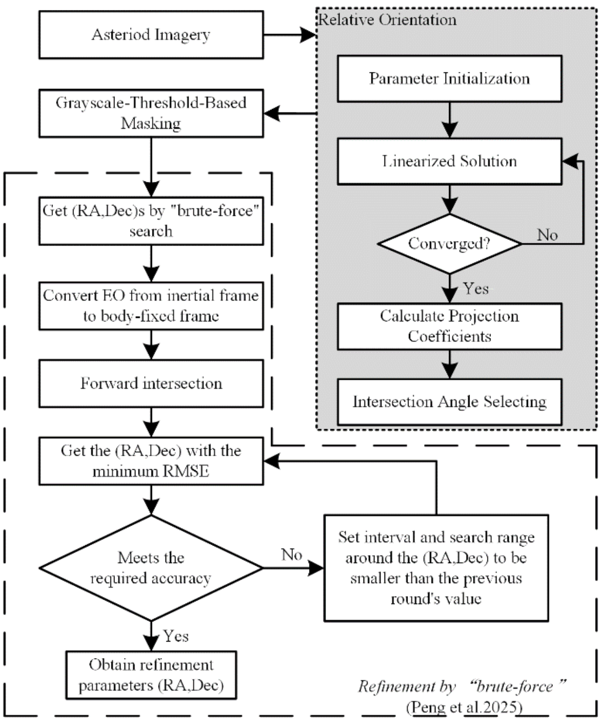

Figure 1 Refinement process for rotation parameters

(RA = right ascension; Dec = declination

2.1 Grayscale-Threshold-Based Masked Feature Matching

During the proximity operations of an asteroid exploration mission, the acquired optical images typically exhibit a stark contrast between the illuminated celestial body and the pitch-black deep-space background. However, relying on a conventional global threshold to isolate the asteroid is often insufficient. (Wang et al., 2025) If left unaddressed, these boundary and noise regions produce a large number of spurious feature points lacking geometric consistency, which severely degrades the accuracy of the subsequent relative orientation and spatial intersection.

$$B(x,y)=\begin{cases}1, & \text{if} I(x,y)\geq T^{*}\\ 0, & \text{if} I(x,y)<T^{*}\end{cases}$$

Due to the aforementioned deep shadows and background stellar noise, $B(x,y)$ typically contains isolated noise patches and internal fragmented holes. To ensure the topological integrity of the mask, a connected component analysis is performed. By extracting the largest connected component C_{max}, scattered background noise is effectively eliminated. Subsequently, a morphological closing operation (dilation followed by erosion) and a hole-filling process are applied to C_{max} to reconstruct a strictly solid target region. The final refined mask $M(x,y)$ is mathematically expressed as:

$$M(x,y)=\text{FillHoles}(C_{max}\blacksquare S)$$

where S represents a predefined morphological structuring element, and $\blacksquare$ denotes the closing operator.

The step-by-step progression of this adaptive masking and morphological refinement process is illustrated in Figure 2. As demonstrated, the initial binary mask generated by the global thresholding inherently contains background noise and internal fragmented holes caused by surface shadows. However, through the subsequent connected component analysis and morphological hole-filling, a topologically complete and noise-free target mask is successfully reconstructed.

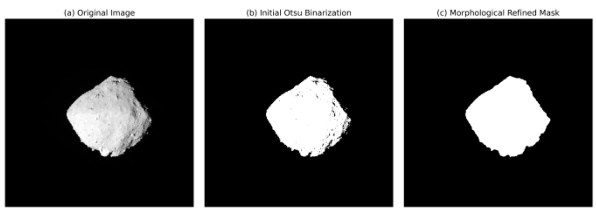

Figure 2 The step-by-step process of the adaptive masking and morphological feature refinement strategy. (a) Original ONC-T image of asteroid Ryugu; (b) Initial binary mask generated by Otsu's thresholding, showing background noise and internal holes; (c) The final topologically complete mask after connected component analysis and morphological hole-filling.

By applying this topologically complete mask $M(x,y)$ to the remote sensing imagery, the Scale-Invariant Feature Transform (SIFT) algorithm (Lowe, 2004) is strictly constrained to operate exclusively within the valid textural region of the asteroid. This targeted extraction not only eliminates the generation of spurious edge features but also dramatically reduces the search space for descriptor matching, thereby yielding a high-precision, outlierfree set of initial tie points for the subsequent geometric processing.

2.2 Stereo Intersection Angle Optimization

During the preliminary phase of an asteroid exploration mission, the absolute exterior orientation parameters of the remote sensing images are typically unknown. Consequently, the 3D reconstruction relies heavily on the geometric configuration of the stereo image pairs (Zhang et al., 2024). When the stereo intersection angle is excessively small, it results in nearly parallel lines of sight from the two cameras. In such ill-conditioned geometric configurations, even a sub-pixel measurement error during feature matching can propagate into substantial positional displacements along the direction of the line of sight (depth uncertainty) (Kirk et al., 2016). To guarantee the reliability of the subsequent parameter estimation, it is imperative to evaluate and optimize the stereo intersection angles before proceeding to the global refinement. The relationship between the stereo intersection angle and the resulting depth uncertainty is geometrically illustrated in Figure 3. As shown in Figure 3 (b), when the intersection angle (λ) is smaller than 5° , the positional error ellipse is severely elongated along the optical ray, thereby dramatically degrading the reliability of the reconstructed spatial point.

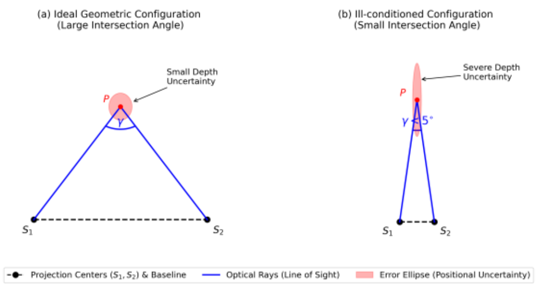

Figure 3 Geometric illustration of positional error propagation based on stereo intersection angles. (a) An ideal geometric configuration with a large intersection angle results in minimal depth uncertainty. (b) An ill-conditioned geometry with an extremely small intersection angle (λ < 5°) drastically elongates the error ellipse, leading to severe depth uncertainty along the line of sight.

The optimization process begins with recovering the relative pose between the paired images. Given a set of highly reliable tie points extracted from the masked regions (as described in Section 2.1), analytical relative orientation is performed. Let $\mathbf{x}_1$ and $\mathbf{x}_2$ be the normalized homogeneous image coordinates of a conjugate point pair. The relative orientation parameters, encapsulated within the Essential matrix E, are iteratively solved based on the epipolar coplanarity condition:

$$\mathbf{x}_1^T E \mathbf{x}_2 = 0$$

where $E = [\mathbf{B}]_\times R_\text{v}$ with R representing the relative rotation matrix and B denoting the relative baseline vector. Upon the successful convergence of the relative orientation, a localized stereo model is established.

Subsequently, spatial forward intersection is executed to determine the 3D model coordinates of the tie points. For any reconstructed 3D point P, the intersection angle γ is defined by the two directional unit vectors, $\mathbf{v}_1$ and $\mathbf{v}_2$, corresponding to the intersecting optical rays from the left and right perspective centers. The angle γ is computed using the dot product formulation:

$$\gamma = \arccos\left(\frac{\mathbf{v}_1 \cdot \mathbf{v}_2}{\| \mathbf{v}_1 \| \| \mathbf{v}_2 \|}\right)$$

To rigorously assess the overall geometric strength of a specific stereo pair, the average intersection angle $\bar{\gamma}$ is calculated across all valid inlier correspondences within that pair. A stringent optimal selection criterion is then enforced: only stereo image pairs exhibiting an average intersection angle strictly greater than a predefined threshold (empirically set to 5° in this study) are retained. Stereo pairs falling below this threshold are systematically discarded, ensuring that the subsequent global rotation parameter refinement is strictly driven by geometric observations with high confidence and minimal depth uncertainty.

2.3 Rotation Parameter Refinement via Iterative Grid Search

With a purified set of feature correspondences and geometrically optimized stereo pairs, the core objective is to determine the precise spin axis orientation-namely, the right ascension (RA, denoted as α) and declination (Dec, denoted as δ). Obtaining these rotational parameters is critical, as they form the mathematical basis for establishing the asteroid's body- fixed coordinate system and enable the rigorous transformation of data from the celestial inertial frame to the body-fixed frame.

For any given candidate set of rotation parameters (α, δ), the exterior orientation (EO) parameters of the involved images are first converted from the inertial frame into the body- fixed frame. The rotation matrix $\mathbf{R}_I^B$, which defines this coordinate transformation, is intrinsically parameterized by the target's pole orientation (α, δ). Following this transformation, spatial forward intersection is executed for all retained optimal stereo pairs. The rigorous imaging geometric model incorporating asteroid rotation parameters is formulated as follows:

$$\begin{bmatrix} X \\ Y \\ Z \end{bmatrix} = \begin{bmatrix} X_S \\ Y_S \\ Z_S \end{bmatrix} + \lambda R_Z(W) R_X(90^\circ - \beta_0) R_Z(\alpha_0 + 90^\circ) R_{Star}^{J2000} R_{Body}^{Star} R_{Cam}^{Body} \begin{bmatrix} x_c \\ y_c \\ -f \end{bmatrix}$$

Because the exact rotational parameters are initially unknown, substituting an approximate (α, δ) pair inevitably introduces discrepancies in the relative poses of the cameras, preventing the conjugate optical rays from intersecting perfectly in 3D space. To quantify these geometrid discrepancies, the Root Mean Square Error (RMSE) of the forward intersection residuals is employed as the objective function for optimization. Let e_i represent the spatial intersection residual for the i -th point. The overall objective function to be minimized is formulated as:

$$RMSE(\alpha, \delta) = \sqrt{\frac{1}{N} \sum_{i=1}^{N} e_i^2}$$

where N is the total number of matched tie points across all geometrically selected stereo pairs.

To systematically locate the global minimum of this objective function and avoid being trapped in local optima due to erroneous initial values, an iterative exhaustive search (i.e., “brute-force” optimization) strategy is implemented. As illustrated in the algorithmic workflow, the process initializes by establishing a 2D parameter search grid spanning a preliminary range of α and δ. The algorithm computes the spatial forward intersection and evaluates the corresponding $RMSE$ for every node within this grid.

Once the node yielding the minimum RMSE is identified, it serves as the central anchor for the subsequent refinement iteration. To progressively achieve higher precision, the search interval (step size) and the search range around this optimal (α, δ) are dynamically adjusted to be strictly smaller than the previous round's values. This coarse-to-fine iterative grid search continues until the predefined accuracy requirement is met, culminating in the final high-precision refinement of the asteroid's rotation parameters.

3. Results

3.1 Experimental Datasets

To validate the effectiveness of the proposed method, remote sensing images of asteroid (162173) Ryugu, acquired by the Hayabusa2 spacecraft during its proximity operations, were selected as the experimental dataset. The 127 images were captured on July 10, 2018, using the ONC-T (Optical Navigation Camera Telescopic) onboard the spacecraft, with a ground resolution of approximately 2.11 meters per pixel (Kameda et al., 2017). These images offer sufficient textural details for high-precision photogrammetric processing (Preusker et al., 2019). Figure 4 shows the images used in the experiment and Table 1 presents the image information.

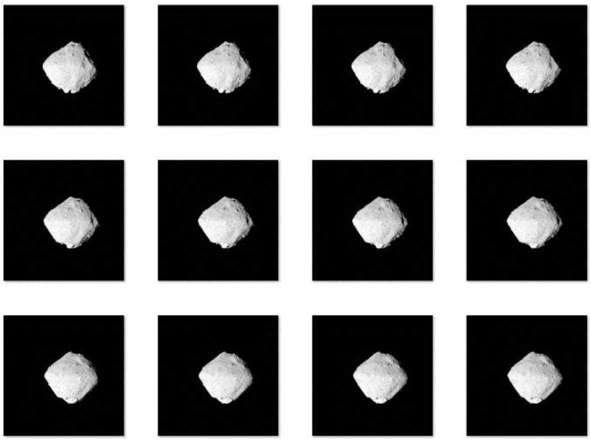

Figure 4 Representative sample images of asteroid Ryugu captured by the Hayabusa2 ONC-T camera.

Table 1 Information of the images selected for experiment.

Parameter	Specification / Value
Spacecraft	Hayabusa2
Instrument	Optical Navigation Camera - Telescopic (ONC-T)
Target Body	Asteroid (162173) Ryugu
Date of Acquisition	July 10, 2018
Number of Images	127
Image Resolution	1024 × 1024 pixels
Field of View (FOV)	6.27° × 6.27°
Ground Sample Distance (GSD)	~ 2.11 m/pixel

3.2 Feature Matching and Stereo Pair Optimization

All selected images were subjected to preprocessing and feature matching to evaluate the impact of the proposed grayscale threshold-based binary masking strategy. A comparative analysis was conducted against a baseline approach that did not employ this masking technique.

Without the masking strategy, the initial unconstrained feature matching yielded 5,174 candidate stereo pairs , from which a total of 548,061 matched points were extracted. Upon applying the RANSAC algorithm to distinguish geometric inliers (correct matches) from outliers (mismatches) , 14,949 points were identified as incorrect matches.

Conversely, the implementation of the grayscale threshold-based masking strategy strictly constrained the matching to the valid asteroid surface. This reduced the number of successfully matched stereo pairs to 3,102. More importantly, the number of mismatched points was significantly reduced to 7,369. The visual comparison of feature matching before and after applying the mask (as shown in Figure 5 and Figure 6) corroborates that the proposed strategy successfully mitigates edge effects and background interference.

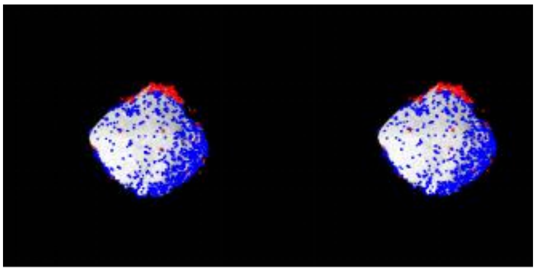

Figure 5 The feature matching results before the application of the masking strategy

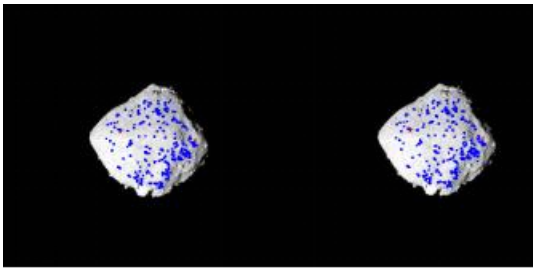

Figure 6 The feature matching results after the application of the masking strategy

Following feature extraction, relative orientation and spatial forward intersection were performed using the precise interior orientation parameters of the ONC-T camera and the matched tie points to calculate the intersection angles. A stringent geometric filter was applied, retaining only those stereo pairs with an intersection angle greater than 5°. This selection process yielded 1,454 optimal stereo pairs containing a total of 137,191 high-quality matched points, which served as the robust data foundation for the subsequent parameter refinement.

3.3 Rotation Parameter Refinement Results

Utilizing the 1,454 geometrically optimized stereo pairs, the iterative "brute-force" refinement process was executed. The objective was to minimize the Root Mean Square Error (RMSE) of the forward intersection residuals.

After four iterative refinement cycles, the rotational parameters for Ryugu successfully converged to a Right Ascension (RA) of 96.5° and a Declination (Dec) of -66.4°. To assess the absolute accuracy of these findings, the results were compared against established reference values (RA = 96.431°, Dec = -66.387°). The proposed method achieved exceptional precision, with errors of merely 0.069° for RA and 0.0126° for Dec. The distribution of RMSE across the search grid during the final iteration is illustrated inFigure 7, and a selection of the corresponding residual values is detailed in Table 2.

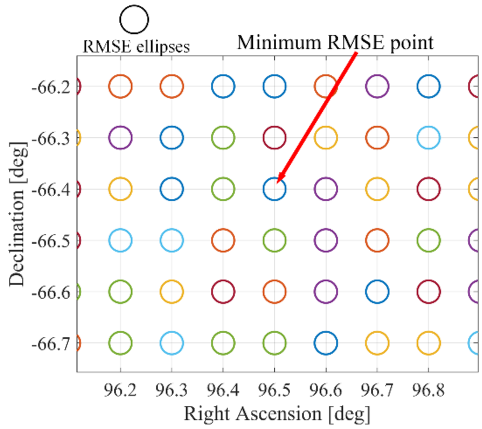

Figure 7 The fourth refinement round of (162173) Ryugu rotation parameters

Table 2 Partial RMSE of forward intersection residuals of fourth round of Ryugu's experiment

RA (°)	Dec (°)	RMSE (pixel)	RA (°)	Dec (°)	RMSE (pixels)
96.4	-66.2	2.186	96.5	-66.6	2.183
96.4	-66.1	2.199	96.5	-66.5	2.176
96.4	-66	2.215	96.5	-66.4	2.173
96.5	-67	2.254	96.5	-66.3	2.175
96.5	-66.9	2.23	96.5	-66.2	2.181
96.5	-66.8	2.21	96.5	-66.1	2.192

To further demonstrate the necessity of the proposed pipeline, a comparative refinement experiment was conducted using the raw matched data (5,174 pairs) without implementing the binary masking and intersection angle selection strategies. The RANSAC algorithm (Fischler and Bolles, 1981) was applied to the same set of selected stereo pairs for a direct comparison. Under these conditions, the estimated parameters converged to RA = 95° and Dec = -67°. These values deviate notably from the reference true values. The clear contrast in accuracy highlights that the proposed integrated strategy achieves two critical improvements: a substantial reduction in mismatched correspondences and a decisive decrease in spatial forward intersection residuals.

4. Discussion

The accurate determination of an asteroid's spin axis is a fundamental prerequisite for establishing a reliable body-fixed coordinate system. The experimental results demonstrate that the proposed pipeline significantly mitigates the inherent challenges of deep-space optical processing. By implementing the grayscale-threshold-based masking strategy, the system effectively isolates the celestial body from the black deep-space background. This step prevents the generation of unstable edge features, ensuring that the feature matching process is strictly confined to valid surface textures. Furthermore, the rigorous selection of stereo pairs without requiring prior knowledge of exterior orientation parameters addresses the critical issue of depth uncertainty. By discarding ill-conditioned geometric configurations (intersection angles less than 5°), the spatial forward intersection avoids severe error propagation along the line of sight.

Beyond merely reducing the RMSE of the intersection residuals, the high-precision rotational parameters derived from this method have profound implications for downstream planetary mapping tasks. Once the body-fixed frame is robustly established using the refined RA and Dec, the generated high-quality tie points and optimized camera poses can be seamlessly ingested into standard planetary photogrammetry suites, such as the USGS ISIS3 bundle adjustment module (Edmundson et al., 2012) or the Ames Stereo Pipeline (Beyer et al., 2018). This facilitates the highly accurate generation of Digital Elevation Models (DEMs) and orthophotos.

5. Conclusions

This paper presents a robust and highly precise refinement method for asteroid rotation parameters, specifically tailored for the proximity operations phase of deep-space exploration missions. The integrated approach leverages a grayscale-threshold binary masking strategy to optimize feature matching and employs stereo intersection angle selection to guarantee geometric strength. Through an iterative "brute-force" search minimizing the spatial intersection residuals, the pole orientation of asteroid (162173) Ryugu was successfully refined.

After four rounds of refinement, the estimated rotational parameters converged to RA = 96.5° and Dec = -66.4°. These results exhibit exceptional accuracy, with deviations of merely 0.069° in RA and 0.0126° in Dec when compared to established reference values. The comparative analysis unequivocally proves that the proposed method significantly reduces mismatched correspondences and effectively minimizes spatial intersection errors. Future work will focus on exploring the integration of these refined rotation parameters as highly accurate priors into a rigorous bundle adjustment model to achieve even further refinement and global consistency.

Acknowledgements

This research was funded by the Space Optoelectronic Measurement and Perception Lab, Beijing Institute of Control Engineering, grant number LabSOMP-2023-07; and the National Natural Science Foundation of China, grant number 42241147; and the Open Program of Collaborative innovation Center of GeoInformation Technology for Smart Central Plains Henan Province, grant number 2023C002.

References

Beyer, R.A., Alexandrov, O., McMichael, S., 2018. The Ames Stereo Pipeline: NASA's Open Source Software for Deriving and Processing Terrain Data. Earth Space Sci. 5, 537–548. https://doi.org/10.1029/2018EA000409

Burmeister, S., Willner, K., Schmidt, V., Oberst, J., 2018. Determination of phobos' rotational parameters by an inertial frame bundle block adjustment. J. Geod. 92, 963–973. https://doi.org/10.1007/s00190-018-1112-8

Drummond, J.D., Fugate, R.Q., Christou, J.C., Hege, E.K., 1998. Full adaptive optics images of asteroids ceres and vesta; rotational poles and triaxial ellipsoid dimensions. Icarus 132, 80–99. https://doi.org/10.1006/icar.1997.5882

Edmundson, K.L., Cook, D.A., Thomas, O.H., Archinal, B.A., Kirk, R.L., 2012. JIGSAW: THE ISIS3 BUNDLE ADJUSTMENT FOR EXTRATERRESTRIAL PHOTOGRAMMETRY. ISPRS Ann. Photogramm. Remote Sens. Spat. Inf. Sci. I–4, 203–208. https://doi.org/10.5194/isprsannals-I-4-203-2012

Folkner, W.M., Dehant, V., Le Maistre, S., Yseboodt, M., Rivoldini, A., Van Hoolst, T., Asmar, S.W., Golombek, M.P., 2018. The rotation and interior structure experiment on the InSight mission to Mars. Space Sci. Rev. 214, 100. https://doi.org/10.1007/s11214-018-0530-5

Jorda, L., Gaskell, R., Capanna, C., Hviid, S., Lamy, P., Ďurech, J., Faury, G., Groussin, O., Gutiérrez, P., Jackman, C., Keihm, S.J., Keller, H.U., Knollenberg, J., Kührt, E., Marchi, S., Mottola, S., Palmer, E., Schloerb, F.P., Sierks, H., Vincent, J.-B., A'Hearn, M.F., Barbieri, C., Rodrigo, R., Koschny, D., Rickman, H., Barucci, M.A., Bertaux, J.L., Bertini, I., Cremonese, G., Da Deppo, V., Davidsson, B., Debei, S., De Cecco, M., Fornasier, S., Fulle, M., Güttler, C., Ip, W.-H., Kramm, J.R., Küppers, M., Lara, L.M., Lazzarin, M., Lopez Moreno, J.J., Marzari, F., Naletto, G., Oklay, N., Thomas, N., Tubiana, C., Wenzel, K.-P., 2016. The global shape, density and rotation of Comet 67P/Churyumov-Gerasimenko from preperihelion Rosetta/OSIRIS observations. Icarus 277, 257–278. https://doi.org/10.1016/j.icarus.2016.05.002

Kameda, S., Suzuki, H., Takamatsu, T., Cho, Y., Yasuda, T., Yamada, M., Sawada, H., Honda, R., Morota, T., Honda, C., Sato, M., Okumura, Y., Shibasaki, K., Ikezawa, S., Sugita, S., 2017. Preflight Calibration Test Results for Optical Navigation Camera Telescope (ONC-T) Onboard the Hayabusa2 Spacecraft. Space Sci. Rev. 208, 17–31. https://doi.org/10.1007/s11214-015-0227-y

Kirk, R.L., Howington-Kraus, E., Hare, T.M., Jorda, L., 2016. THE EFFECT OF ILLUMINATION ON STEREO DTM QUALITY: SIMULATIONS IN SUPPORT OF EUROPA EXPLORATION. ISPRS Ann. Photogramm. Remote Sens. Spat. Inf. Sci. III–4, 103–110. https://doi.org/10.5194/isprsannals-III-4-103-2016

Kuppa, K., McMahon, J., Dietrich, A., 2022. Initial pole estimation using infrared imagery 1–2.

Lowe, D.G., 2004. Distinctive Image Features from Scale-Invariant Keypoints. Int. J. Comput. Vis. 60, 91–110. https://doi.org/10.1023/B:VISI.0000029664.99615.94

Müller, T.G., Ďurech, J., Ishiguro, M., Mueller, M., Krühler, T., Yang, H., Kim, M.-J., O'Rourke, L., Usui, F., Kiss, C., Altieri, B., Carry, B., Choi, Y.-J., Delbo, M., Emery, J.P., Greiner, J., Hasegawa, S., Hora, J.L., Knust, F., Kuroda, D., Osip, D., Rau, A., Rivkin, A., Schady, P., Thomas-Osip, J., Trilling, D., Urakawa, S., Vilenius, E., Weissman, P., Zeidler, P., 2017. Hayabusa-2 mission target asteroid 162173 Ryugu (1999 JU3): Searching for the object's spin-axis orientation. Astron. Astrophys. 599, A103. https://doi.org/10.1051/0004-6361/201629134

Peng, Z., Geng, X., Zhang, J., Wang, Y., 2025. Preliminary refinement of rotation parameters of asteroids based on photogrammetric processing of on-orbit remote sensing images. Int. Arch. Photogramm. Remote Sens. Spat. Inf. Sci. XLVIII-G-2025, 1181–1187. https://doi.org/10.5194/isprs-archives-XLVIII-G-2025-1181-2025

Preusker, F., Scholten, F., Elgner, S., Matz, K.-D., Kameda, S., Roatsch, T., Jaumann, R., Sugita, S., Honda, R., Morota, T., Tatsumi, E., Cho, Y., Yoshioka, K., Sawada, H., Yokota, Y., Sakatani, N., Hayakawa, M., Matsuoka, M., Yamada, M., Kouyama, T., Suzuki, H., Honda, C., Ogawa, K., 2019. The MASCOT landing area on asteroid (162173) Ryugu: Stereo-photogrammetric analysis using images of the ONC onboard the Hayabusa2 spacecraft. Astron. Astrophys. 632, L4. https://doi.org/10.1051/0004-6361/201936759

Preusker, F., Scholten, F., Matz, K.-D., Roatsch, T., Willner, K., Hviid, S.F., Knollenberg, J., Jorda, L., Gutiérrez, P.J., Kührt, E., Mottola, S., A'Hearn, M.F., Thomas, N., Sierks, H., Barbieri, C., Lamy, P., Rodrigo, R., Koschny, D., Rickman, H., Keller, H.U., Agarwal, J., Barucci, M.A., Bertaux, J.-L., Bertini, I., Cremonese, G., Deppo, V.D., Davidsson, B., Debei, S., Cecco, M.D., Fornasier, S., Fulle, M., Groussin, O., Güttler, C., Ip, W.-H., Kramm, J.R., Küppers, M., Lara, L.M., Lazzarin, M., Moreno, J.J.L., Marzari, F., Michalik, H., Naletto, G., Oklay, N., Tubiana, C., Vincent, J.-B., 2015. Shape model, reference system definition, and cartographic mapping standards for comet 67P/Churyumov-Gerasimenko – Stereo-photogrammetric analysis of Rosetta/OSIRIS image data. Astron. Astrophys. 583, A33. https://doi.org/10.1051/0004-6361/201526349

Thomas, P.C., Binzel, R.P., Gaffey, M.J., Storrs, A.D., Wells, E.N., Zellner, B.H., 1997. Impact Excavation on Asteroid 4 Vesta: Hubble Space Telescope Results. Science 277, 1492–1495. https://doi.org/10.1126/science.277.5331.1492

Wang, Yifan, Yan, X., Xie, H., Yang, M., Ye, Z., Wang, Yaqiong, Chen, H., Chen, J., Ying, T., Tong, X., 2025. Shape reconstruction and rotation axis estimation of small bodies using a voxel-divided shape-from-silhouette method. Geo-Spat. Inf. Sci. 1–27. https://doi.org/10.1080/10095020.2025.2596193

Watanabe, S., Hirabayashi, M., Hirata, N., Hirata, Na., Noguchi, R., Shimaki, Y., Ikeda, H., Tatsumi, E., Yoshikawa, M., Kikuchi, S., Yabuta, H., Nakamura, T., Tachibana, S., Ishihara, Y., Morota, T., Kitazato, K., Sakatani, N., Matsumoto, K., Wada, K., Senshu, H., Honda, C., Michikami, T., Takeuchi, H., Kouyama, T., Honda, R., Kameda, S., Fuse, T., Miyamoto, H., Komatsu, G., Sugita, S., Okada, T., Namiki, N., Arakawa, M., Ishiguro, M., Abe, M., Gaskell, R., Palmer, E., Barnouin, O.S., Michel, P., French, A.S., McMahon, J.W., Scheeres, D.J., Abell, P.A., Yamamoto, Y., Tanaka, S., Shirai, K., Matsuoka, M., Yamada, M., Yokota, Y., Suzuki, H., Yoshioka, K., Cho, Y., Tanaka, S., Nishikawa, N., Sugiyama, T., Kikuchi, H., Hemmi, R., Yamaguchi, T., Ogawa, N., Ono, G., Mimasu, Y., Yoshikawa, K., Takahashi, T., Takei, Y., Fujii, A., Hirose, C., Iwata, T., Hayakawa, M., Hosoda, S., Mori, O., Sawada, H., Shimada, T., Soldini, S., Yano, H., Tsukizaki, R., Ozaki, M., Iijima, Y., Ogawa, K., Fujimoto, M., Ho, T.-M., Moussi, A., Jaumann, R., Bibring, J.-P., Krause, C., Terui, F., Saiki, T., Nakazawa, S., Tsuda, Y., 2019. Hayabusa2 arrives at the carbonaceous asteroid 162173 ryugu—a spinning top–shaped rubble pile. Science 364, 268–272. https://doi.org/10.1126/science.aav8032

Zhang, J., Geng, X., Yu, J., Liu, J., Liu, P., Peng, Z., Ma, X., Wang, Q., Wang, Yinhui, Wang, Yuying, 2024. A Rapid Method for Match Pair Determination and Optimal Image Selection from Disordered and Massive Asteroid Images. https://doi.org/10.20944/preprints202411.1452.v1